Jurnal Teknologi

Full Paper

NUMERICAL ANALYSIS OF DENSITY-DRIVEN FLUCTUATION IN GROUNDWATER CAUSED BY SALTWATER INTRUSION

Makoto Kawabata, Junichiro Takeuchi*, Masayuki Fujihara

Water Resources Engineering, Division of Environmental Science & Technology, Graduate School of Agriculture, Kyoto University, Kyoto, Japan

Article history
Received
15 July 2015
Received in revised form
2 August 2015
Accepted
26 August 2015

*Corresponding author
takejun@kais.kyoto-u.ac.jp

Graphical abstract

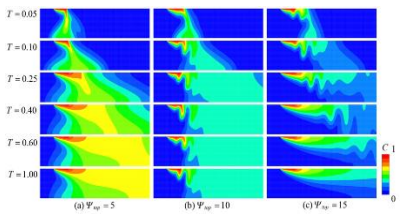

Abstract

Density-driven flow in groundwater environment is concerned with various fields such as saltwater intrusion in coastal areas, groundwater contamination due to non-aqueous phase liquid from garbage disposal plants, and designing of geothermal utilization systems. It is important to appropriately consider density-driven flow when dealing with these objectives, because density-driven flow changes solute and heat distribution as well as groundwater flow. In recent years, salt damage to farmlands caused by storm surge or tsunami is a serious problem. In order to prevent salt damage to crops, salt is often leached intentionally by freshwater. However, the effect of leached saltwater on groundwater environment is not considered adequately. It is known that flow instability is caused by unignorable density difference between intruding saltwater and groundwater. This instability changes groundwater flow and salinity distribution, and sometimes produces fluctuant flow that keeps oscillating. Therefore, it is important to comprehend these phenomena for management of groundwater resources. The purpose of this study is to ascertain the condition in which flow instability occurs when saltwater intrudes into groundwater. Systematic numerical experiments were conducted to specify a subdomain where flow keep oscillating in a parameters space. The equations governing groundwater flow and solute transport were discretized spatially by the Galerkin finite element method and temporally by the Crank-Nicolson method. The obtained results showed that the oscillatory flow depends not only on Rayleigh number concerning density difference and permeability, but also on both of basal groundwater flow and saltwater intrusion rates.

Keywords: Rayleigh number, saltwater intrusion, numerical experiment, attractor reconstruction

1.0 INTRODUCTION

Density-driven flow is the fluid flow caused by density gradient attributed to variations in solutes and/or heat, which changes the flow directions of solute and/or heat as well as fluid flow. It could occur in groundwater if some conditions are satisfied, and it has a great effect on solute and/or heat transports. Hence, it is significant to specify the condition for occurrence of density-driven flow and to understand the dynamics of it from the point of view of water resource management.

It is known that density-driven flows in groundwater are associated with various phenomena. Saltwater intrusion in coastal areas is a typical example, in which saltwater wedge is formed by the density difference between saltwater and fresh water [1]. Groundwater contamination due to non-aqueous phase liquids (NAPLs) is also a well-known example. In a case of light NAPLs, they move almost vertically and spread along water flow after arriving at water table. On the other

hand, dense NAPLs leaked from ground surface infiltrate in vertical direction, and form oil sump after arriving at groundwater table [2].

In the cases of density-driven flow caused by temperature difference, it is shown that flow instability emerges by specific conditions [3, 4]. Simmons *et al.* (2001) conducted and reviewed the numerical experiments concerned with variable density flow instability in heterogeneous porous media [5]. Their numerical results indicates that both the onset of instabilities and subsequent growth and decay are intimately related to the structure and variance of the permeability field.

In recent years, the flood risk due to storm surges or high tides by frequent extreme events has been increasing [6]. Storm surges often cause salt damage to crops in farmlands in the coastal areas. In order to prevent the damage by saltwater, it is recommended to leach salt intentionally by freshwater [7]. However, in such cases, the dynamics of leached saltwater into groundwater is not considered adequately. Therefore, this study is intended to clarify the impact of saltwater intrusion on groundwater flow through systematic numerical experiments, and to specify the conditions for raising instable flow in a parameters space.

2.0 GOVERNING EQUATIONS

In this study, a vertical two dimensional coordinate system where x and z are the horizontal and vertically upward directions, respectively is used. For the sake of brevity, the governing equations are transformed into dimensionless version here. The derivation of the governing equations are based on Holzbecher (1998) [1].

The dimensionless version of the governing equation for groundwater flow with variable water density is described with the stream function under following assumptions: incompressibility of water, rigidity of the aquifer, absence of sources or sinks, and the Boussinesq approximation.

$$\frac{\partial}{\partial X}\left(\frac{\mu^r}{\kappa_z^r}\frac{\partial \Psi}{\partial X}\right)+\frac{\partial}{\partial Z}\left(\frac{\mu^r}{\kappa_x^r}\frac{\partial \Psi}{\partial Z}\right)=Ra\frac{\partial C}{\partial X} \tag{1}$$

with

$$Ra=\frac{H\Delta\rho g\kappa_0}{\mu_0 D}, \tag{2}$$

$$(U,W)^T=\left(\frac{\partial \Psi}{\partial Z},-\frac{\partial \Psi}{\partial X}\right)^T, \tag{3}$$

$$C=\frac{c-c_{\min}}{c_{\max}-c_{\min}}, \tag{4}$$

where X and Z are the dimensionless coordinates for x and z, respectively; Ψ is the dimensionless stream function; Ra is the Rayleigh number; μ^r is a relative value of the viscosity of water μ based on the representative viscosity μ_0, μ is given by $\mu=\mu^r\mu_0$; κ_x^r and κ_z^r are relative values of the intrinsic permeability in the x and z directions based on the representative intrinsic permeability κ_0, respectively, where the intrinsic permeability κ_x and κ_z are given by $\kappa_x=\kappa_x^r\kappa_0$ and $\kappa_z=\kappa_z^r\kappa_0$, respectively; C is the dimensionless salinity; H is the representative length, which is the height of an objective domain in this study; g is the gravitational acceleration, D is the dispersion coefficient; U and W are the dimensionless velocity in the X and Z directions, respectively; the water density ρ is given by $\rho(C)=\rho_f+C\Delta\rho$ where ρ_f is freshwater density, $\Delta\rho$ is the difference of density between freshwater ($\rho(1)$) and saltwater ($\rho(0)$); c is the salinity; $c_{\max}$ and $c_{\min}$ are the maximum and minimum salinity in the domain, respectively.

The dimensionless version of the governing equation for solute transport is described as follows.

$$\phi R\frac{\partial C}{\partial T}=\frac{\partial}{\partial X}\left(\phi\frac{\partial C}{\partial X}\right)+\frac{\partial}{\partial Z}\left(\phi\frac{\partial C}{\partial Z}\right)-\left(U\frac{\partial C}{\partial X}+W\frac{\partial C}{\partial Z}\right) \tag{5}$$

where ϕ is the porosity of the porous media, R is the retardation factor, T is the dimensionless time.

3.0 NUMERICAL EXPERIMENTS

In this section, the settings for the numerical experiments are described. The objective domain is assumed to be a shallow aquifer, in which groundwater flows horizontally unless saltwater intrudes. Through the boundary conditions, a constant vertical saltwater intrusion into groundwater from a part of the ground surface is given.

3.1 Boundary and Initial Conditions

The boundary conditions for groundwater flow and salt transport are given as illustrated in Figure 1. The objective domain is presumed as a rectangle, and it has a saltwater intrusion zone on the top. In regard to the stream function, the top and bottom are set as the Dirichlet-type boundary condition, while both sides of the domain are set as the Neumann-type. Constant values Ψ_{top} and $\Psi_{top}+\Psi_{ent}$ is given to the top except for the saltwater intrusion zone, in which a value linearly changing from Ψ_{top} to $\Psi_{top}+\Psi_{ent}$ is given, and zero is given to the bottom. To the sides of the domain, $\partial\Psi/\partial\boldsymbol{n}=0$ is imposed, where $\boldsymbol{n}$ is the unit normal vector to the boundary. The basal groundwater flow rate and the saltwater intrusion rate are modulated by the values of Ψ_{top} and Ψ_{ent}, respectively. This boundary condition allows groundwater to flow freely across the side boundaries, and not to flow across the top and bottom boundaries except for the salt water intrusion zone. Regarding the salinity, the Dirichlet-type boundary condition where the value is unit is given to the intrusion zone, and the Neumann-type boundary condition where $\partial C/\partial\boldsymbol{n}=0$ is given to the other boundaries. As an initial condition for the stream function, a uniform flow without any saltwater intrusion, i. e., $\Psi_{ent}=0$ is given. Besides, the salinity in the whole domain is zero as an initial state.

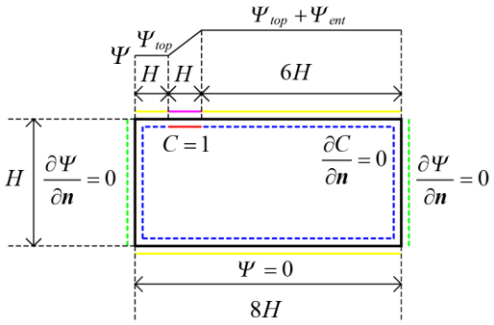

Figure 1 Boundary conditions

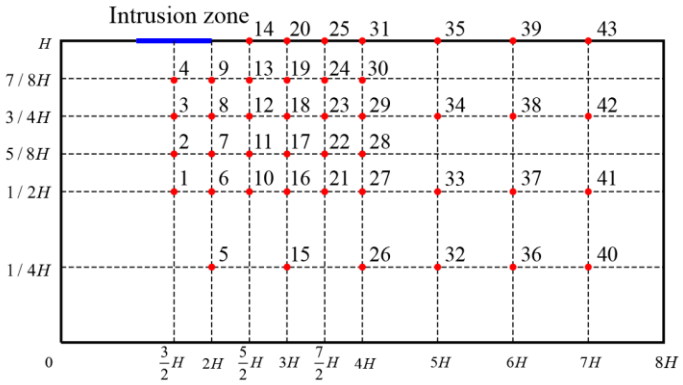

Figure 2 Sampling points

3.2 Computational Settings

The objective domain is divided into triangular elements based on an equally-spaced 40×320 regular mesh. The computational mesh consists of 13,161 nodes and 25,600 elements. The time step of the simulations is 10^{-3} (dimensionless time), and $T_{\max}$, which is the ending time, is set as 2 or less if the state becomes steady. The domain is assumed to be homogeneous, isotropic, and isothermal, and so all the parameters representing a relative value κ_x^r, κ_z^r, and μ^r are taken as unit. Similarly, the height of the domain H and the retardation factor R are also given as unit. The porosity of the domain is given as 0.35.

For the numerical experiments, various values are given to three variables: the Rayleigh number Ra, and the Dirichlet-type boundary values Ψ_{top} and Ψ_{ent} for the stream function. The Rayleigh number varies from 50 to 150 at 25 intervals, and Ψ_{top} from 5 to 20 at 5 intervals. Ψ_{ent} has three candidates as 0.1, 1, and 5. Basically, as the combination of these three variables, sixty simulations are conducted to investigate a condition for fluctuation phenomena in this study.

3.3 Analysis Method

To evaluate each computational result quantitatively, some sampling points are picked up among the computational nodes. The number of the sampling points is 43 as illustrated in Figure 2. Moving variance of a time series data of salinity calculated at each point is monitored, and whether the flow fluctuates or not is determined by the maximum values among the sampling points after sufficient time elapses.

In addition, behaviors of the salinity at the sampling points are analyzed with the attractor reconstruction, which is a non-linear-data analysis technique. In the data analysis, the dynamics in a 2-D phase space is reconstructed from a single time series data, using a time delay, where a time series data is transformed into a trajectory in the 2-D phase space. The coordinates of the trajectory are defined as $(C(t),C(t+\tau))$, where τ (>0) is the time delay. Generally, the trajectory of a time series oscillating forms a circle, when the time delay is given as one fourth of its cycle. If the time delay is larger or smaller than one fourth of the cycle, the trajectory gets to an ellipse. Moreover, the trajectory ultimately becomes a line on the diagonals when the delay is half of the cycle or the cycle itself. Therefore, the time delay is given so as to enlarge a circle made by a trajectory in this study. On the other hand, when the time series is convergent, the trajectory approaches a certain point.

4.0 COMPUTATIONAL RESULTS

4.1 Behaviors of Intruding Saltwater

Through the above-mentioned analyses, this study found that the behaviors of the intruding saltwater could be divided into the following three patterns: (1) rapid convergence without oscillation, (2) oscillation, and (3) oscillatory convergence. Figure 3 shows the typical examples of the three patterns, in which time series distributions of salinity are delineated. The computational settings is common ($Ra=100$, $\Psi_{ent}=1$) among the three computations except for the basal groundwater flow, where Ψ_{top} is given as 5, 10, and 15 to the left, middle, and right columns, respectively. It is found from Figure 3 that the salinity distributions get to steady states without and with oscillation in the left and right columns, respectively, and that the salinity distribution keeps oscillating in the middle column. Figure 4, which illustrates time varying salinity at the sampling point 9 (Figure 2), evidences these three different patterns. With a careful observation, it is noticed that the oscillatory pattern ($\Psi_{top}=10$) changes from a period-1-type oscillation (a simple harmonic oscillation) to a period-2-type oscillation after the time passes about 0.15. Figure 5 also evidences these three patterns, where the time delay τ is set as 0.004. It is found that the trajectories of the rapid (5-(a)) and oscillatory (5-(c)) convergences approach a respective point, which is a stable fixed point, and that the trajectory of the oscillation (5-(b)) have a limit cycle with a double circle.

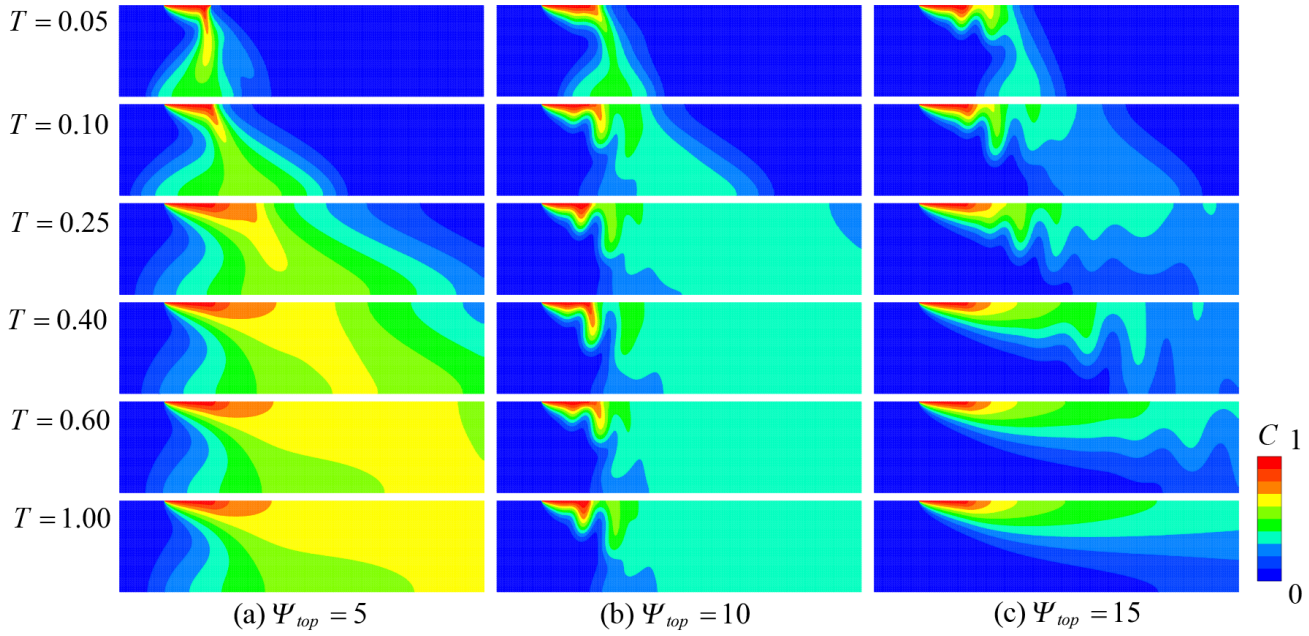

Figure 3 Time variations of saline distribution $(Ra = 100, \Psi_{ent} = 1)$

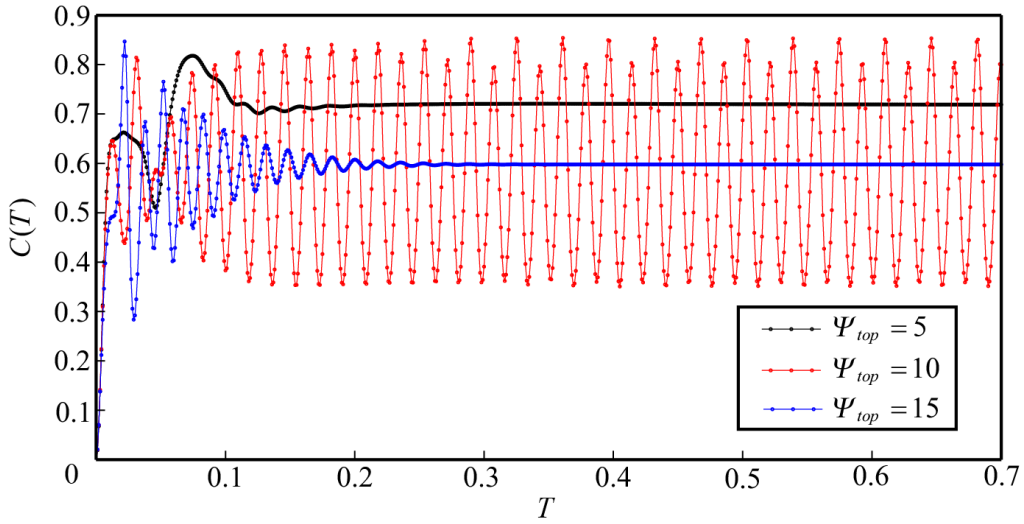

Figure 4 Time variations of salinity at sampling point 9 in the case of $Ra = 100$, $\Psi_{ent} = 1$, and $\Psi_{top} = 5, 10, 15$

Among other combinations of the three parameters, a period-1-type oscillation is found in a computational setting ($Ra = 75$, $\Psi_{top} = 10$, and $\Psi_{ent} = 1$), and the temporal change of salinity and the trajectory in a phase space at the sampling point 21 are shown in Figures 6 and 7, respectively. The trajectory that approaches a simple limit cycle in a case of $\tau = 0.007$ is illustrated in Figure 7.

These results show the extinction of a stable fixed point and the occurrence of a limit cycle (the change from the rapid convergence to the oscillation); and the recurrence of a fixed point and the extinction of the limit cycle (the change from the oscillation to the oscillatory convergence) as the basal groundwater flow increases. These indicate that some bifurcations occur depending on the basal groundwater flow rate, and that period-doubling also occurs if a simple limit cycle is formed before the limit cycle with a double circle. However, it is difficult at present to specify the location where such transformations of fixed points occur, since only relatively sparse points in a three-parameter space (Ra, Ψ_{top}, and Ψ_{ent}) were investigated in this study.

4.2 The Condition For Flow Instability

Although available information is limited since saltwater behaviors are evaluated only at relatively sparse points in the three-parameter space, a rough sketch of classification in the space could be obtained. Table 1 shows the maximum variances among the sampling points at the end of each computation, in conjunction

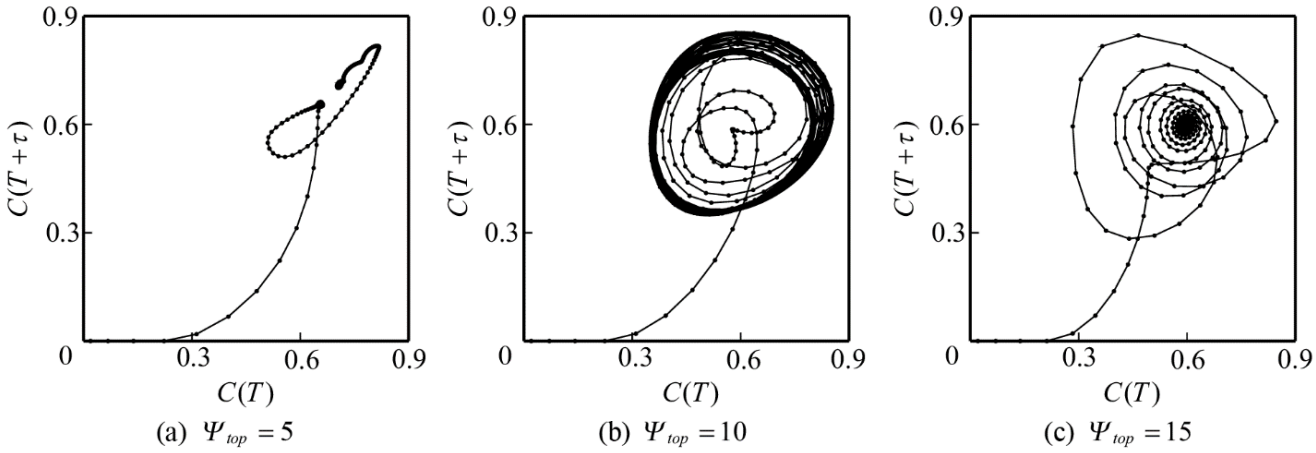

Figure 5 Trajectories in phase space ($Ra=100$ and $\Psi_{ent}=1$)

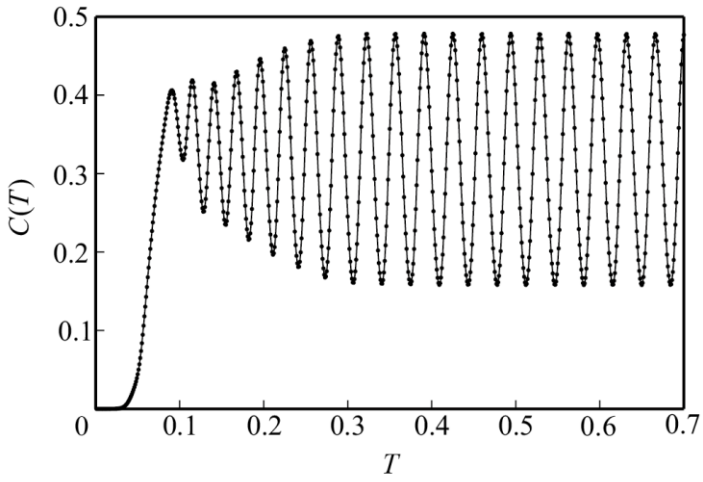

Figure 6 Time variation of salinity ($Ra=75, \Psi_{top}=10,$ and $\Psi_{ent}=1$)

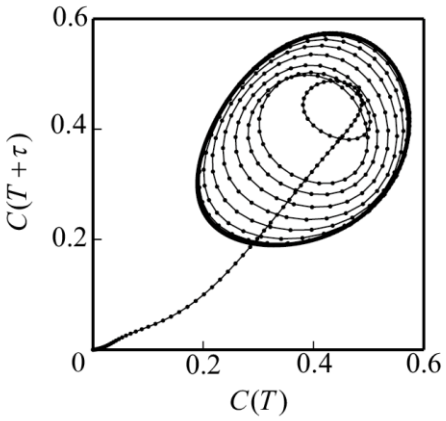

Figure 7 Trajectory in phase space ($Ra=75, \Psi_{top}=10,$ and $\Psi_{ent}=1$)

with the classification regarding the three-behavior patterns. The green, yellow, and pink cells represent the rapid convergence, the oscillation, and the oscillatory convergence patterns, respectively. The yellow cells have relatively large variance, and the green and pink cells have almost zero variance, which implies the salinity is convergent in the cells. From these tables, the following three tendencies are found. (1) While the green subdomains in these tables do not change, the yellow subdomains expand as the saltwater intrusion rate (i.e., Ψ_{ent}) increases. (2) As the Rayleigh number increases, the behavior of intruding salinity changes from the rapid convergence pattern to the oscillatory convergence pattern, and further changes into the oscillation patterns. (3) As the basal groundwater flow rate (i.e., Ψ_{top}) increases, the behavior typically changes from the rapid convergence pattern to the oscillation pattern, and further to the oscillatory convergence pattern, which is shown in the previous subsection. However, this is not always true in some parts where the yellow subdomain does not intrude adequately or where green subdomains are not seen in the row of $\Psi_{top}=5$.

Table 1 The maximum variance of temporal saline variation at the sampling points

$\Psi_{ent} = 0.1$		Rayleigh number				
		50	75	100	125	150
Ψ_{top}	5	2.50E-13	2.37E-9	8.28E-08	9.20E-07	9.75E-07
	10	6.55E-30	2.39E-13	3.23E-02	3.72E-02	2.98E-02
	15	2.79E-30	4.47E-30	9.03E-30	3.45E-02	3.34E-02
	20	1.04E-29	8.37E-30	6.00E-30	5.46E-30	3.50E-02

$\Psi_{ent} = 1$		Rayleigh number				
		50	75	100	125	150
Ψ_{top}	5	1.28E-13	2.50E-10	1.89E-08	6.75E-07	7.74E-07
	10	6.55E-30	1.32E-02	2.94E-02	3.92E-02	3.18E-02
	15	1.04E-29	1.19E-29	7.14E-30	3.47E-02	3.56E-02
	20	6.55E-30	6.00E-30	7.14E-30	1.11E-29	3.58E-02

$\Psi_{ent} = 5$		Rayleigh number				
		50	75	100	125	150
Ψ_{top}	5	7.82E-14	6.97E-14	3.59E-10	2.47E-07	1.03E-06
	10	1.27E-29	3.40E-02	4.25E-02	4.46E-02	3.49E-02
	15	9.71E-30	1.43E-29	3.07E-02	3.25E-02	4.03E-02
	20	7.74E-30	1.11E-29	1.25E-30	2.53E-02	2.75E-02

Rapid convergence Oscillatory convergence Oscillation

5.0 CONCLUSION

In this study, oscillatory phenomena of vertically intruding saltwater into horizontally flowing groundwater are investigated through numerical experiments, where the Rayleigh number, the basal groundwater flow rate, and the saltwater intrusion rate are varying parameters.

From the obtained results, three different patterns: the rapid convergence, the oscillation, and the oscillatory convergence, are found in behavior of intruding saltwater. These three patterns were shown by time variations of spatial salinity distributions, time series of salinity at a certain point, and trajectory in a 2-D phase space. From the trajectories, it is indicated that a stable fixed point changes to an unstable fixed point, and changes to a stable fixed point again, as the groundwater flow rate increases. Therefore, the three-parameter space of the Rayleigh number, the basal groundwater flow rate, and the saltwater intrusion rate are divided into subdomains with respect to which intruding pattern occurs. From the obtained result, the occurrence of the oscillatory flow does not depend only on the Rayleigh number, but also on both the basal groundwater flow rate and the saltwater intrusion rate. To identify the location of the onset and extinction of the oscillatory behavior, meticulous investigation is needed.

Acknowledgement

This research was partially funded by an international travel grant No.68 from JSIDRE academic fund.

References

[1] Holzbecher, E. 1998. *Modeling Density-Driven Flow in Porous Media*. Springer. 1-47.

[2] Tamai, Y. and Honma, S. 2012. Experiments and Analysis on the Simultaneous Seepage of Pore-Water and Oils in Soils. *Proceedings of the School of Engineering of Tokai University*. 52(2): 217-224. In Japanese.

[3] Holzbecher, E. and Yusa, Y. 1994. Numerical Experiments on Free and Forced Convection in Porous Media. *Int. J. Heat Mass Transfer*. 38(11): 2109-2115.

[4] Yoshimura, Y., Takeuchi, J. and Fujihara, M. 2013. Analysis of Effects on Groundwater Flow by Infiltration-Water Temperature. *Proceedings of the Japanese Society for Irrigation, Drainage, and Rural Engineering*. 140-141. In Japanese.

[5] Simmons, C. T., Fenstemaker, T. R. and Sharp Jr J. M. 2001. Variable-Density Groundwater Flow and Solute Transport in Heterogeneous Porous Media: Approaches, Resolutions and Future Challenges. *Journal of Contaminant Hydrology*. 52: 245-275.

[6] Nicholls, R. J., Hoozemans, F. M. J. and Marchand, M. 1999. Increasing Flood Risk and Wetland Losses Due to Global Sea-Level Rise: Regional and Global Analysis. *Global Environmental Change*. 9: 69-87.

[7] Rural Development Bureau, The Ministry of Agriculture, Forestry and Fisheries. 2011. *The Manual of the Desalination for the Agricultural Land.* In Japanese.